Research Article

Journal of Environmental Nanotechnology

Multifaceted Analysis of L-Alanine-Doped Creatininium Benzene Sulphonate Single Crystals for Optical Modulation Application

C. Ramajeya* and K. Balasubramanian

PG and Research Department of Physics, The M.D.T. Hindu College (Affiliated to Manonmaniam Sundaranar University), Tirunelveli, TN, India

Received: 02.07.2024 Accepted: 29.08.2024 Published: 30.09.2024

*ramajeya1983@gmail.com

ABSTRACT

Creatininium Benzene Sulphonate (CBS) and L-Alanine-doped Creatininium Benzene Sulphonate (ACBS) single crystals were grown using the slow evaporation technique. Xpert HighScore software was utilized to determine lattice parameters including Full Width at Half Maximum (FWHM), crystallite size, and lattice strain. Fourier transform infrared spectroscopy was used to identify the functional groups present in the samples. The thermal properties of CBS and ACBS crystals were analyzed using Thermogravimetric and Differential Thermal Analysis. Optical properties including optical conductivity, extinction coefficient, and refractive index were measured using UV-Vis spectroscopy. The mechanical characteristics of both samples were studied using Vicker's microhardness testing, and the dielectric response was recorded for various frequencies. The second harmonic generation values of samples were compared to those of potassium dihydrogen phosphate. Overall, CBS and ACBS crystals demonstrate promising characteristics as sustainable materials for optical modulation. Incorporating amino acids, such as L-Alanine, enhances the photoconductive properties of the crystals by improving charge carrier mobility and reducing recombination rates, resulting in more efficient optical modulation. This study explores the impact of doping single crystals with amino acids on their optoelectronic and dielectric properties for potential applications in optical modulation devices. Specifically, this research investigates the role of L-Alanine, a zwitterionic amino acid, in enhancing the performance of CBS single crystals, with the aim of optimizing their structural, thermal, optical, and mechanical properties for optical modulation. These findings highlight the potential of amino acid-doped single crystals in advancing optical devices, driving innovations in optoelectronics and photonics.

Keywords: Creatininium benzene sulphonate; L-Alanine; Dielectric constant; SHG optical modulation.

1. INTRODUCTION

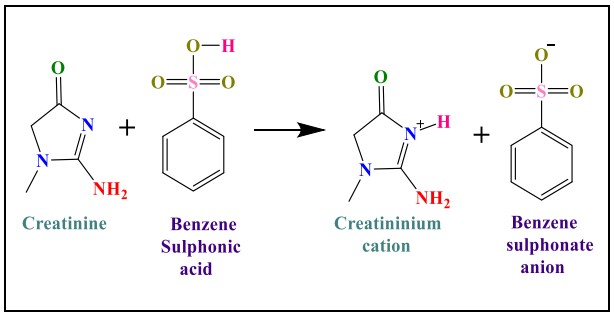
While a reduction in second harmonic generation (SHG) efficiency might seem like a drawback, the unique properties introduced by amino acid doping offer potential benefits that can enhance existing applications in the field of photonics. Leveraging the distinct properties of amino acids, doping single crystals can significantly enhance their functionality and broaden their applications across various fields, including optoelectronics, photonics, electronics, and biomedicine. Amino acid doping improves the dielectric properties of crystals, enhancing charge distribution and polarization characteristics, thereby boosting their performance in electronic and dielectric applications. Additionally, amino acid-doped crystals can be employed in antifouling coatings for biomedical implants, preventing microbial adhesion and biofilm formation. By modifying the refractive index, these doped crystals can be tailored for specific optical devices (Matsui *et al.* 2019; Wang *et al.* 2020; Yauri *et al.* 2023). Doping also enhances the mechanical strength and durability of single crystals, making them more resistant to mechanical stress and wear. Zwitterions, such as those found in amino acids, play a significant role in the crystal growth process by promoting nucleation, improving crystal quality, controlling growth rates, managing solubility and supersaturation, modifying lattice parameters, enhancing functional properties, and ensuring biocompatibility. These roles make them valuable in synthesizing high-quality crystals for a wide range of applications.

Devices that use light to control the flow of signals are typically used for routing optical signals in telecommunication networks. Zwitterion doping in single crystals offers several benefits crucial for developing and optimizing optical modulation devices (Ananda Kumari *et al.* 2020; Durgababu *et al.* 2021). By enhancing the structural, optical, and dielectric properties of the crystals, zwitterionic dopants enable the fabrication of high-performance materials suitable for advanced optoelectronic, photonic, and biomedical applications. Devices that modify the amplitude, phase, or polarization of light are essential for applications in fiber optics and signal processing. Integrated circuits that use light for carrying and processing signals, enable

compact and efficient optoelectronic devices. Thus, the suitability of L-Alanine, an amino acid with zwitterionic properties, to enhance dielectric and optical applications in CBS single crystals has been studied, revealing its potential as a candidate for optical modulation devices.

2. SYNTHESIS

A single crystal of CBS can be synthesized by mixing the precursors creatinine and benzene sulphonic acid. The solution evaporation technique was utilized under a constant temperature, using double-distilled water as the solvent. Super-saturated solutions are critical in synthesizing single crystals because they facilitate nucleation, control solubility and crystal growth, enhance crystal quality, enable seeding and growth manipulation, and ensure reproducibility in experimental outcomes. Thus, the equimolar supersaturated solutions of creatinine and benzene sulphonic acid were mixed to form a homogeneous mixture, which was left to dry at room temperature. After an induction period of approximately 14 days, small, transparent crystals began to grow in the beaker. Eventually, after 40 days, high-quality single crystals of CBS were formed, as shown in Fig. 1a. Additionally, 0.5 to 1 mol percent of L-Alanine was added to the CBS solution, resulting in the synthesis of ACBS single crystals (Fig. 1b).



3. RESULTS AND DISCUSSION

3.1 Powder X-ray Diffraction

The powder XRD (PXRD) patterns were recorded for both CBS and ACBS crystals. Crystal lattice data for CBS are shown in Table1. The indexed XRD pattern of CBS is shown in Fig. 2a, while the indexed XRD pattern of ACBS is shown in Fig. 2b.

Knowledge of interstitial sites is essential in material design and engineering. It allows researchers to tailor the properties of materials by introducing dopants into interstitial sites, thereby modifying characteristics such as conductivity, catalytic activity, or optical properties. The structural information is listed in Table 2. Compared to ACBS 0.5, ACBS 1 shows more peaks, confirming its higher crystalline nature. All the sharp peaks are labelled using hkl indices. As the FWHM decreases, the crystallite size increases, as shown in Table 2.

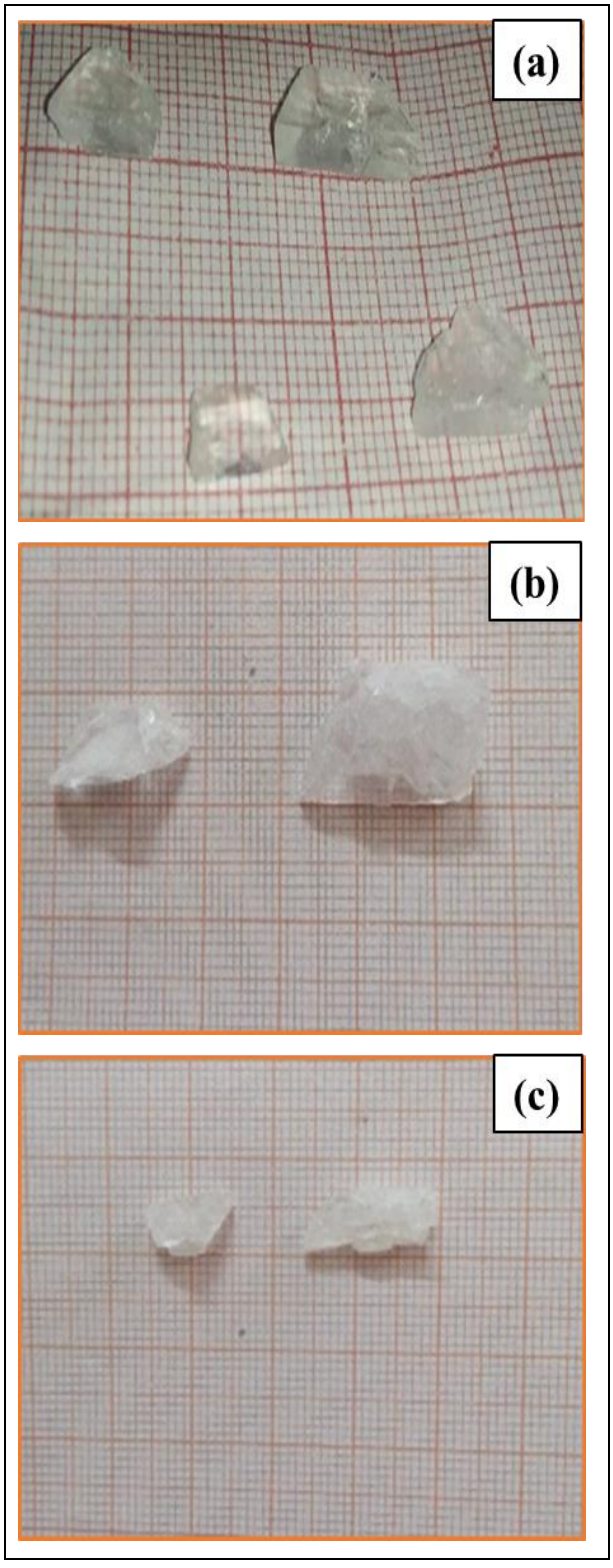


Fig. 1: (a) Creatininium Benzene Sulphonate (CBS) single crystal, (b) 0.5% and (c) 1% L-Alanine doped Creatininum benzene sulphonate (ACBS) single crystal

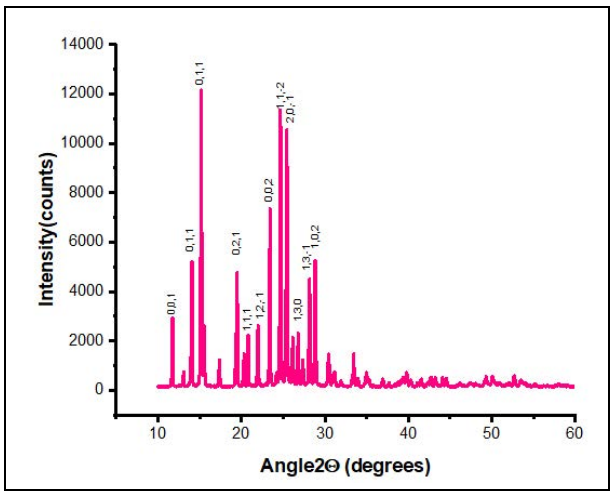


Fig. 2a: XRD pattern of CBS

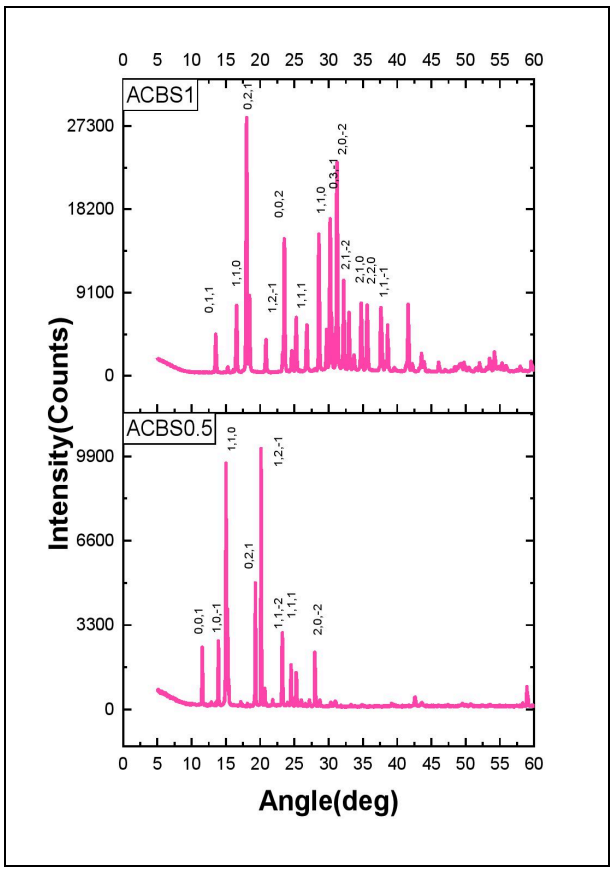


Fig. 2b: XRD pattern of ACBS

Table 1. Crystal lattice data for CBS

Empirical Formula Crystal system	$C_{10}H_{13}N_3O_4S$ Monoclinic
a(Å)	7.0354
b(Å)	11.4990
c(Å)	7.8480
α(°)	90.00
β(°)	102.34
γ (°)	90.00
V (Å3)	634.90
Space group	P_{21}

Table 2. Structural refinement parameters of ACBS and CBS

Structural property	CBS	ACBS 0.5	ACBS 1
FWHM	0.2205	0.11692	0.05623
Crystallite size	472.92 nm	625	862
Lattice strain	0.2418%	0.22%	0.21%

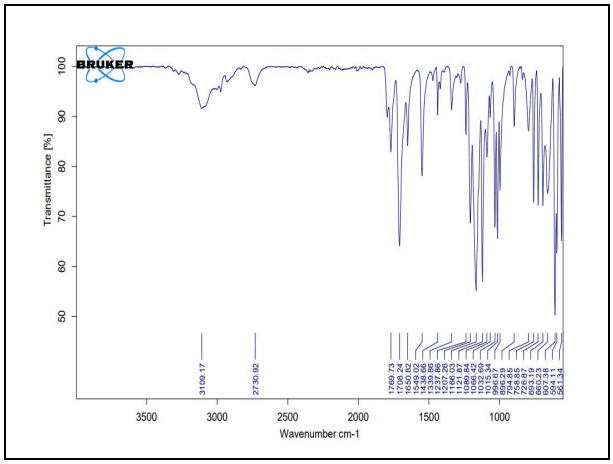


Fig. 3a: FTIR of CBS single crystal

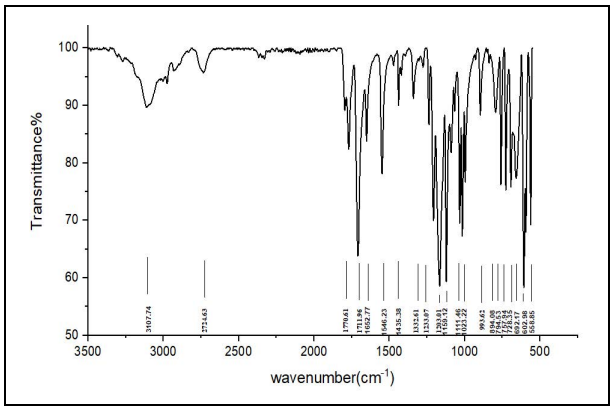


Fig. 3b: FTIR of ACBS single crystal

3.2. FTIR Analysis

The presence of creatininium cations is confirmed by detecting the C=O stretching vibration at 1760 cm^{-1} in FTIR, which is closer to the calculated wavenumber of approximately 1822 cm^{-1}. Peaks at 1696 cm^{-1} and 1563 cm^{-1} correspond to C-H bending and NH_2 bending vibrations, respectively, with theoretical values expected at 1639 cm^{-1} for C-H bending and 1565 cm^{-1} for NH_2 bending. The C-H bending vibration is identified at 1431 cm^{-1} in FTIR, with the calculated mode observed at 1420 cm^{-1}. Additionally, the C-H stretching vibration appears at 880 cm^{-1}. Confirmation of the presence of benzene sulfonic acid is based on peaks at 1017 cm^{-1}, which align with the theoretical value of 1021 cm^{-1}, indicating symmetric S=O stretching vibrations. The C-C stretching vibrations are observed at 1036 cm^{-1}, with the calculated value expected around 1024 cm^{-1}. The C-

H bending vibration of substituted benzene, theoretically expected at 1318 cm^{-1}, corresponds to the actual vibration at 1322 cm^{-1}. A strong peak at 733 cm^{-1}, matching the theoretical value of 704 cm^{-1}, confirms the interaction of the amino acid with creatininium benzene sulfonic acid. Fig. 3a and 3b depict the FTIR spectra of CBS and ACBS single crystals.

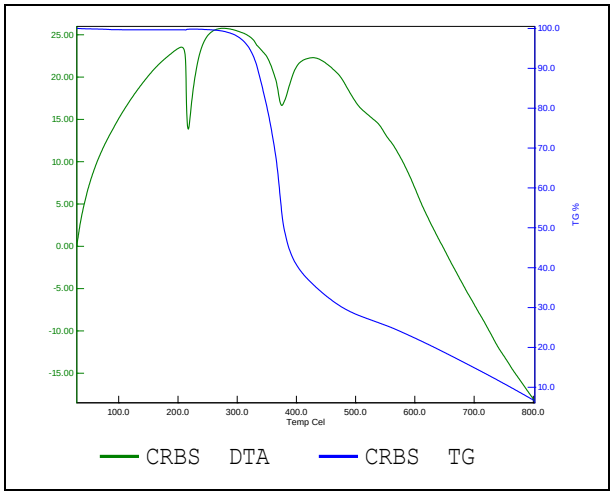


Fig. 4(a): TG/DTA for CBS

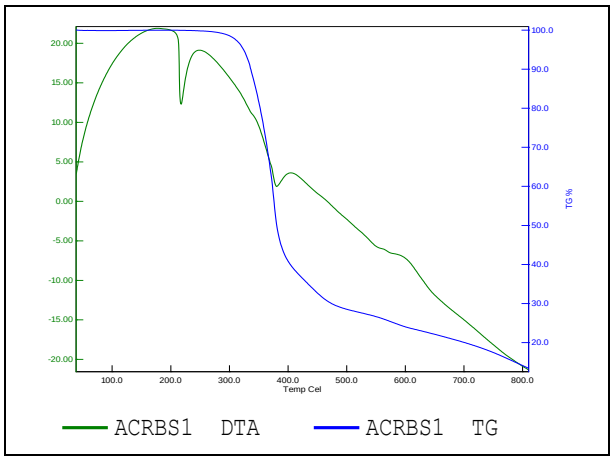


Fig. 4(b): TG/DTA for ACBS 1

3.3 Thermogravimetry Differential Thermal Analysis or TG/DTA

The TG/DTA analysis of the CBS single crystal was conducted over the temperature range 0–800°C, with the TG and DTA curves shown in Fig. 4a. The TG curve illustrates the decomposition process of the CBS single crystal, where significant weight loss is observed between 330–450 °C, indicating the decomposition of all functional groups present in the sample. The DTA curve at 210°C demonstrates that the material remains thermally stable up to this temperature and DTA curve shows two endothermic peaks with phase changes. This thermal stability is essential for the design of nonlinear optical (NLO) materials (Durgababu *et al.* 2021; Wang *et al.* 2023; Tian *et al.* 2023; Sahaya *et al.* 2023; Kiran *et al.* 2024). Both CBS and ACBS 1, display thermal stability, as shown in Fig. 4a and 4b.

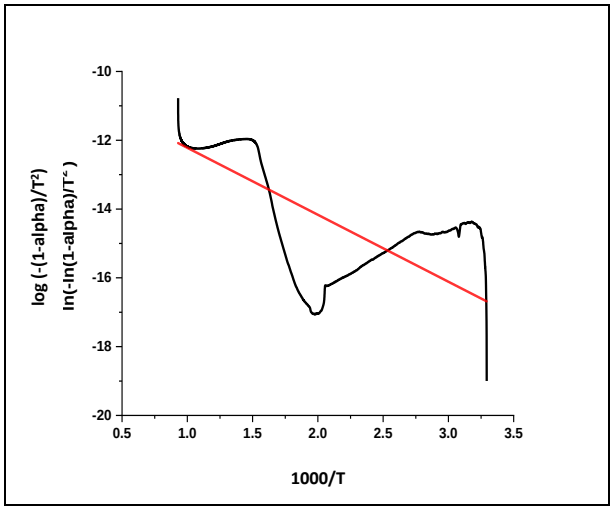


Fig. 4(c): The graph to find the activation energy of CBS

The Differential Thermal Analysis (DTA) curve provides data on the transformations that have occurred in the sample, such as glass transitions, crystallization, melting and sublimation. By analyzing these peaks and deviations on the DTA curve, one can identify and quantify the temperatures and enthalpies associated with these transformations, providing insight into the thermal properties and behavior of the material. In CBS, the phase changes (glass transition, crystallization, melting, and sublimation) with constant enthalpy are observed. This implies fluctuations in the enthalpy (total heat content) of the system throughout these transformations. Since Fig. 4c provides four values of activation energy for CBS, this equilibrium can be challenging to achieve and maintain in a real-world scenario and would suggest a complex interplay of simultaneous thermal events within the material. From the slope value, activation energy, enthalpy and free energy were calculated for CBS. In the same way, in ACBS, each of these transformations is characterized by specific peaks or deviations on the DTA curve, allowing for the identification and quantification of the temperatures and enthalpies associated with these processes. The detailed analysis of these transformations provides valuable insights into the thermal properties, stability, and behavior of the material.

The activation energy graphs for ACBS 0.5 and ACBS 1 are shown in Fig. 4d and Fig. 4e, respectively. Negative entropy can be utilized in engineering applications such as signal processing, where it is used to remove noise and improve signal quality.

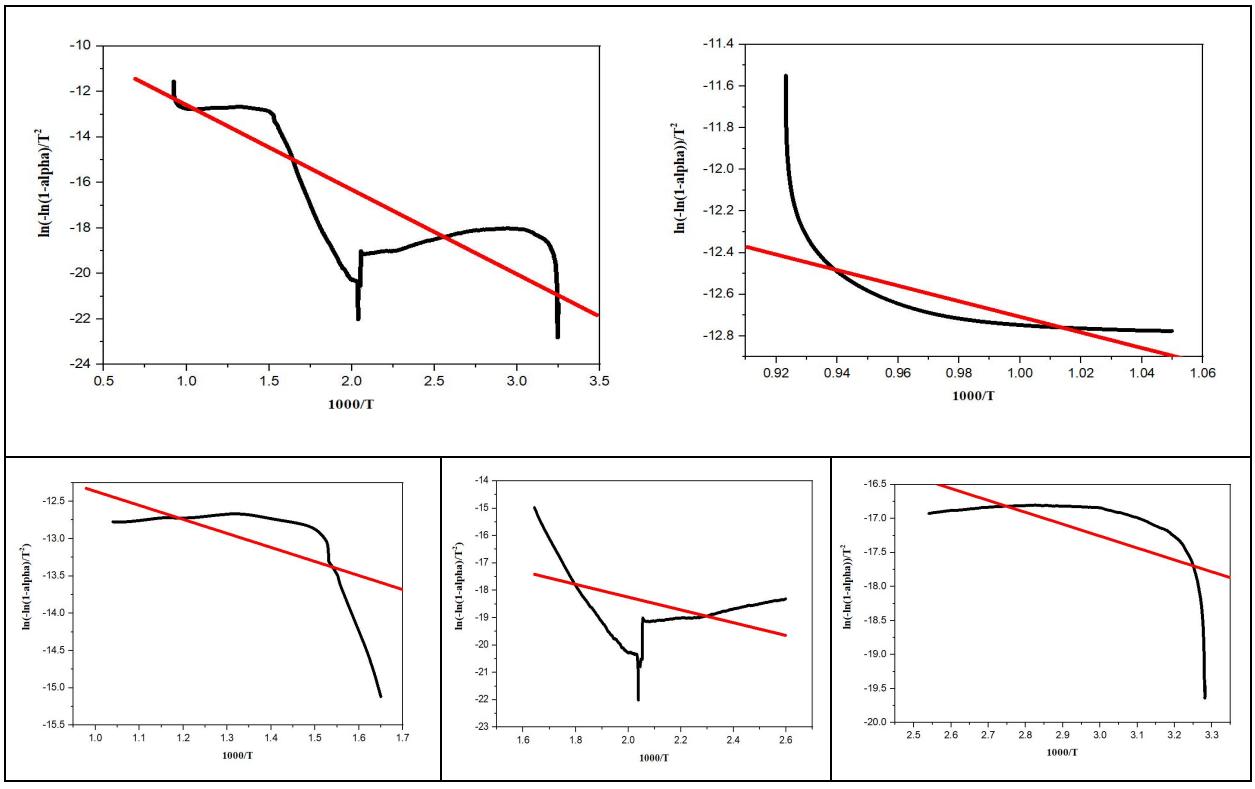
Thus, ACBS samples with this expected entropy can be used for device fabrication. This implies that the sample absorbs heat during phase transitions or

decomposition, which can affect its thermal stability. Higher enthalpy values might indicate that more energy is required to destabilize the material, implying greater stability (Rao *et al.* 2016; Henning *et al.* 2018; Aslfattahi *et al.* 2019; Shi *et al.* 2021; Atinafu *et al.* 2022). The slope values of four different phases of all samples are listed in Table. 3 were calculated using Coats-Redfern method. From the table we observe that good thermal stability after doping is benificial for fiber optic devices and optical modulators.

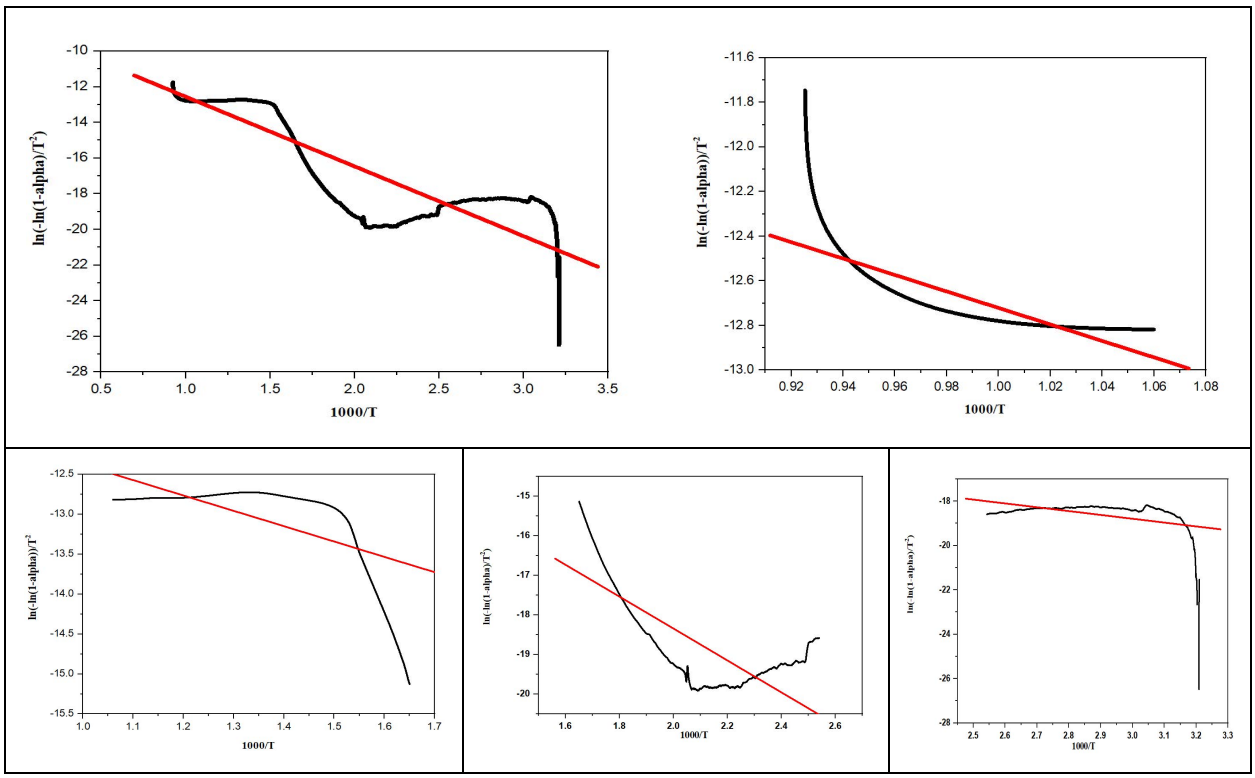
3.4 UV Analysis

By plotting $(\alpha h\nu)^2$ versus $h\nu$, the direct optical bandgap of the CBS crystal was estimated, as shown in Fig. 5a. Here, g is the optical bandgap, A is a constant, $h\nu$ represents the energy of photon, and α represents the optical absorption coefficient. Since there is no significant absorption between 500-1000 nm in Fig. 5b, this range is suitable for optoelectronic and energy conversion devices (Feng *et al.* 2015; Jubu *et al.* 2020; Klein *et al.* 2023). By extrapolating the linear portion of the graph, E_g was determined. The second linear portion in UV Tauc plot shows secondary phase transitions due to the electronic cloud present in both samples. Since they are not affecting bulk properties, only the first linear portion was used to determine the bandgap. The absorption at 236.91 nm indicates π-π* transition (Gu *et al.* 2021; Kiran *et al.* 2024). The transmittance spectra of both CBS and ACBS, shown in Fig. 5c, also confirm their cutoff wavelength at 236.91Hz. The optical conductivity of ACBS 1, ACBS 0.5 and CBS are shown in Fig. 5d. The Tauc plots of the samples are displayed in Fig. 5e. The increased optical conductivity observed with doping can have specific applications. For example, in devices where optical modulation or signal processing is required, high optical conductivity is crucial for efficient light transmission or absorption.

The simultaneous presence of peaks in both refractive index (Fig. 5f) and extinction co-efficient graphs (Fig. 5g) indicates a specific wavelength where the material interacts strongly with light, both in terms of absorption and refraction. This could be due to electronic transitions within the material or resonance effects at that wavelength. The peak in the extinction coefficient graph indicates wavelengths where ε is highest, implying strong absorption or scattering of light by the material at those wavelengths. Therefore, a higher extinction coefficient value at a particular wavelength indicates that the material absorbs light more effectively at that wavelength, corresponding to a peak in the graph.



4(d): The graph to find the activation energy of ACBS 0.5



4(e): The graph to find the activation energy of ACBS 1

Table 3. Thermal parameters at different phases

Phase	Temp in 1000/T	Slope	E_a (J)	Entropy = R* ln (Ah/KT) (J/mol/K)	Enthalpy (J/mol)	Free energy (J)
	CBS					
Phase 1	0.9925	1.752	14566.13	-242.19	6189.274	250216.8
Phase 2	1.5075	0.5145	4277.79	-232.743	-1237.37	153153.2
Phase 3	1.9555	0.3124	2598.04	-200.873	-1653.57	101068.8
Phase 4	3.230	0.1207	1003.58	-195.706	-1570.43	59020.3
	ACBS 0.5					
Phase 1	0.958800	3738.73	31083.80	-248.570	22412.550	281663.60
Phase 2	1.504750	1846.38	15350.80	-230.340	9825.651	162898.70
Phase 3	1.897450	4078.85	33911.56	-222.390	29529.890	146738.70
Phase 4	3.128083	2064.70	17165.92	-195.340	14508.100	76953.68
	ACBS 1					
Phase 1	0.958890	3690.26	30680.82	-248.161	22010.380	280810.80
Phase 2	1.497620	1920.90	15970.36	-230.582	10418.890	164385.10
Phase 3	2.085030	4035.94	33554.81	-217.710	29567.330	133983.40
Phase 4	3.131320	1725.89	14349.05	-186.854	11693.940	71366.84

This peak signifies good absorption characteristics of the material at that specific wavelength (Fig. 5g). In spectroscopic analysis, this correlation can be important for understanding the optical behavior of materials, especially in designing optical devices where absorption and refraction properties are critical. Observing the same peak at the same wavelength in both the extinction coefficient and refractive index graphs indicates a wavelength where the material exhibits significant optical activity (Bassett *et al.* 2019; Tailor *et al.* 2021; Li *et al.* 2022; Sánchez *et al.* 2023; Zallo *et al.* 2023).

3.5 Microhardness Analysis

The hardness values, denoted as "Hv" were determined by applying various indentation loads, labeled as "P" ranging from 25 g to 100 g, using a

Diamond Pyramidal indenter in a Vickers microhardness tester. The Hv values were calculated using the formula $1.855P/d^2$, where "d" represents the diagonal length in millimeters. By plotting a graph that connects the logarithm of P versus the logarithm of d, we can derive the Hardness number "n". The calculated hardness numbers, ranging from 2.3 to 3.9, identify the materials as soft. For CBS and ACBS, the Mayer index numbers were found, as illustrated in Fig. 6. Hence, both materials are suitable for the fabrication of optoelectronic devices (Ilbay *et al.* 1994; Rao *et al.* 2020; Chandra Kandpal *et al.* 2021).

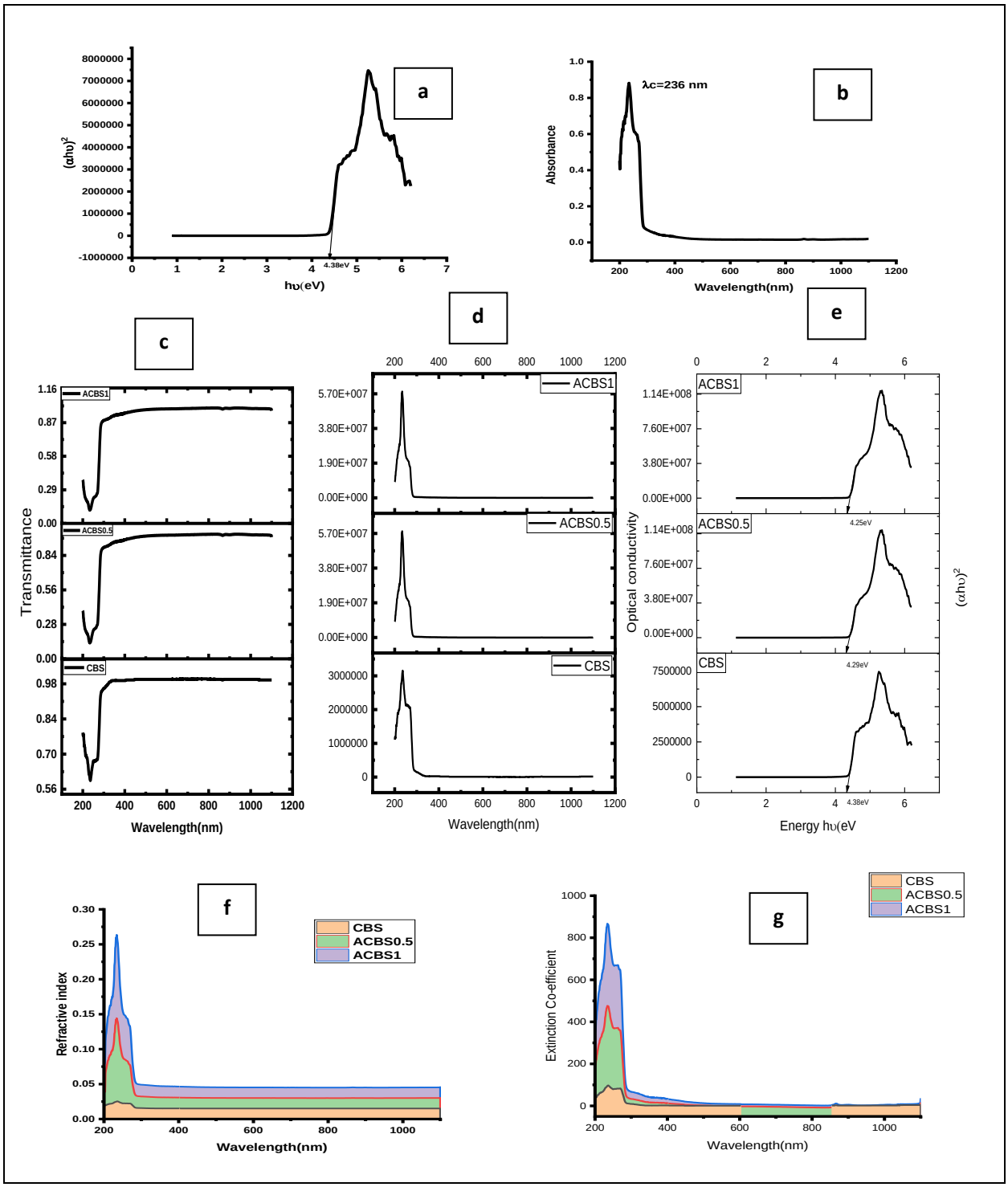


Fig. 5: (a) Tauc plot of CBS (b) The absorption spectrum of CBS (c) Transmittance of CBS, ACBS 0.5 and ACBS 1 (d) Optical conductivity of CBS, ACBS 0.5 and ACBS 1 (e) Tauc plot of CBS, ACBS 0.5 and ACBS 1 (f) Refractive index value from 0.02 to 0.05 upon doping (g) Comparison of Extinction co-efficient

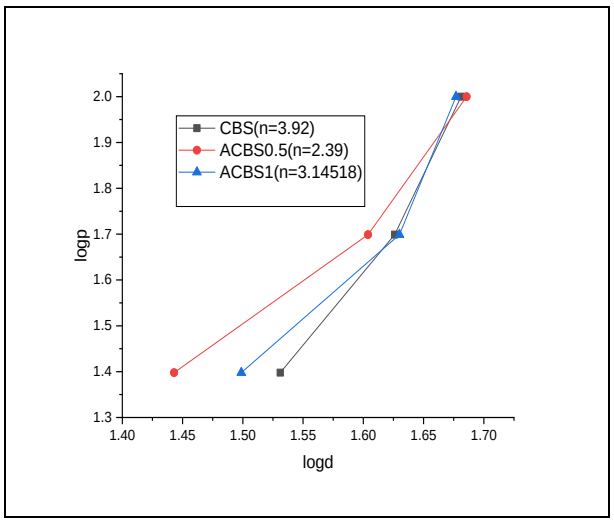


Fig. 6: Plot showing hardness numbers of CBS and ACBS single crystals

A slope value above 2 in log P versus log d plot indicates that the relationship between the applied load (or pressure) and deformation follows a power law with an exponent of 2. This suggests a relatively ramp increase in load with increasing deformation, which has implications for the material's mechanical properties and behavior under stress. Understanding this relationship is crucial for applications in material science, fracture mechanics, and engineering design.

3.6 Dielectric Studies

Dielectric constant and dielectric loss are two major distinct properties of a material depending on its nature. Improved electronic properties with dielectric properties (e.g., high dielectric constant and low loss) can enhance the efficiency and performance of opto-modulated devices (Matthias *et al.* 1948; Purushothaman *et al.* 2021). When the dielectric constant remains constant at higher frequencies, it suggests that the material's ability to store and release electrical energy remains predictable and does not vary significantly with the frequency of the electric field. Dielectric constant at various frequencies and dielectric loss in CBS and ACBS single crystal samples are illustrated in Fig. 7a and Fig. 7b, respectively.

In practical terms, a constant dielectric constant at high frequencies is desirable in applications such as RF and microwave communication systems, antennas, radar systems, and high-speed data transmission cables. It ensures that the material provides consistent electrical characteristics across the entire frequency spectrum of interest, thereby maintaining signal integrity and reliability in electronic devices and systems operating at higher frequencies. A steeper dielectric loss versus log f graph indicates that the material dissipates more energy at higher frequencies, which can affect its performance in electronic and communication applications requiring low loss characteristics. In photonic integrated circuits, materials with low dielectric loss and suitable electronic properties ensure efficient signal transmission and minimal energy loss, leading to better performance in optical communication networks.

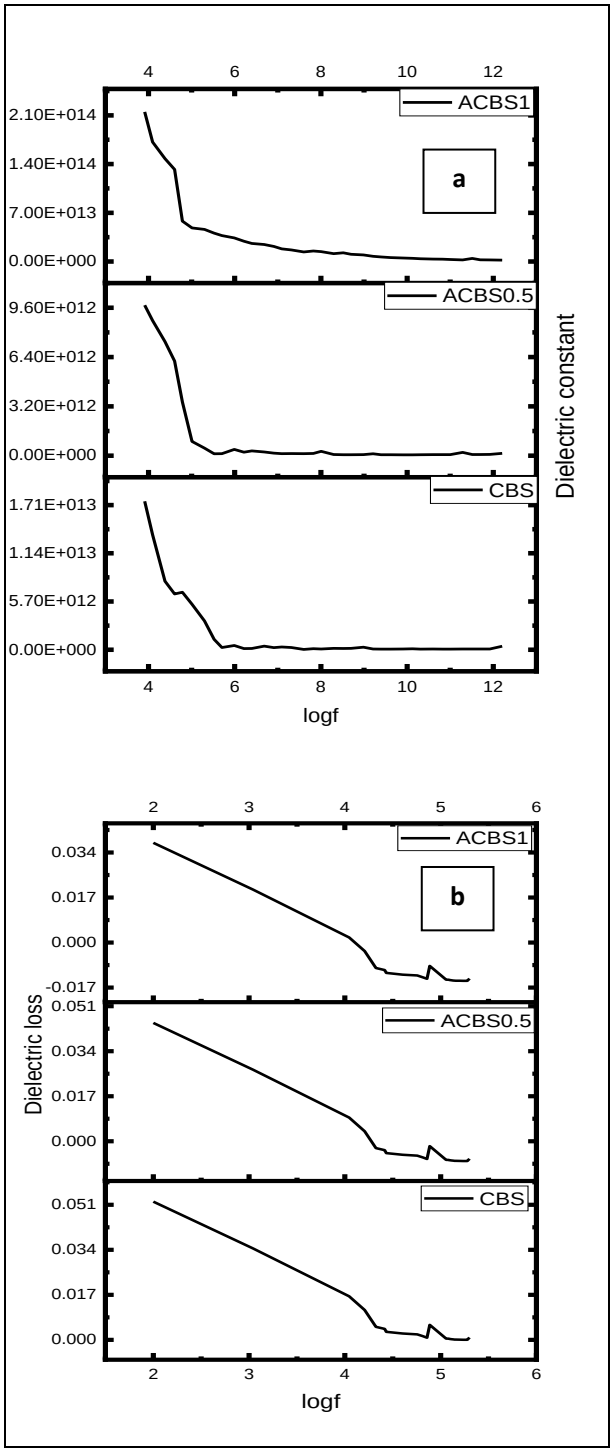


Fig. 7: (a) Variation of dielectric constant for various frequencies (b) Dielectric loss in CBS and ACBS single crystal

3.7 Second Harmonic Generation

The modified Kurtz-Perry technique is a versatile method for estimating the conversion efficiency of nonlinear optical materials in SHG. Nd:YAG laser radiation with a pulse width of 5 ns and a fundamental wavelength of 1064 nm was used to expose a powder sample of CBS and ACBS single crystals. The predominant emission of green light at 532 nm confirms the presence of SHG in the sample. Using KDP as the reference material with an output energy of 7.5 mJ and an input energy of 0.5 J, the SHG efficiency of the CBS crystal was found to be 0.746 times that of KDP. The SHG efficiencies of ACBS 0.5 and ACBS1 were found to be 0.5733 and 0.4533 times that of KDP, respectively. Doping a single crystal to decrease SHG can be advantageous in devices that require precise control over optical signals. In essence, doping single crystals with amino acids can alter their optical properties in complex ways, enhancing optical conductivity while diminishing SHG efficiency. Understanding and controlling these effects are essential for leveraging such materials in various advanced optoelectronic applications (Chakaravarthy *et al.* 2023).

By reducing SHG, one can manipulate the intensity or wavelength of the generated second harmonic signal. This can be useful in optical modulation devices used in telecommunications and signal processing Therefore, CBS and ACBS single crystals can be recognized as nonlinear materials suitable for the fabrication of optoelectronic devices (Purusothaman *et al.* 2023).

3.8 Laser Damage Threshold (LDT)

The LDT values are crucial for both transmissive and reflective optical elements, as well as in applications where laser-induced modification or destruction of a material is the desired outcome. The LDT study for CBS and ACBS crystals was conducted under identical experimental conditions using a Q-switched pulsed Nd (1064 nm) laser beam operating in transverse mode (TM00) with a pulse width of 10 ns and a frequency of 10 Hz. The output laser beam, with a diameter of 1 mm, was irradiated on the crystal surface. The crystal was positioned at the focus of a converging lens with a focal length of 10 cm. The pulse energy of the input laser beam was measured using a power meter (QUANTA ray model no: 170-10). The energy density was calculated using the expression for power density $P = E/\tau (\pi r^2)$, where E is the input energy density in mJ, τ is the pulse width in ns, and r is the radius of the circular spot in mm. The CBS and ACBS crystals exhibited high laser damage threshold values of 2.95 GW/cm² and 4.471 GW/cm², respectively, which are significantly higher than those of KDP (0.20 GW/cm²) and urea (1.50 GW/cm²) crystals. Due to its high LDT, it is useful for high power laser applications. A good laser damage threshold value for optical modulation devices meets or exceeds the maximum expected laser power levels in the application, ensuring reliable and safe operation without risk of damage from laser exposure (Ananda Kumari *et al.* 2020; Ramesh *et al.* 2020).

4. CONCLUSION

Characterization techniques are crucial for assessing the quality and purity of grown crystals, ensuring they possess the desired properties and are suitable for their intended applications. Impurities or defects can significantly impact the crystals performance. Comprehensive analyses were done, including XRD, FTIR, UV-Vis, Vickers hardnesss test, TG/DTA, SHG measurements and LDT. Parameters such as FWHM, crystallite size, and lattice strain were compared. Optical and NLO characterizations revealed that increased optical conductivity with reduced SHG upon doping can be advantageous in applications where minimizing NLO effects is desired, such as in certain types of sensors or optical communication systems. Reduced bandgap after doping confirms its increase in optical conductivity. Absorption and refraction at the same wavelength are essential for optimizing performance, particularly in optical modulation devices, where having both absorption and refraction at the same wavelength allows for precise control over how light is transmitted, reflected, or modulated. Amino acids can modify the refractive index and other optical properties of materials, allowing for tunable optical devices. These changes can be exploited in devices where precise control of optical properties is needed, such as in tunable lasers, optical filters, and variable optical attenuators. Higher enthalpy accounts for the thermal stability of ACBS single crystals. Additionally, the very high laser damage threshold values in both CBS and ACBS crystals make them ideal for use in high-power laser applications. Mechanical hardness also remains good even after doping. The results indicate that L-Alanine doping significantly improves optical conductivity while reducing SHG efficiency, suggesting a relationship between non-linear optical properties and enhanced transparency and conductivity suitable for optical modulation.

FUNDING

This research received no specific grant from any funding agency in the public, commercial, or not-for-profit sectors.

CONFLICTS OF INTEREST

The authors declare that there is no conflict of interest.

COPYRIGHT

This article is an open-access article distributed under the terms and conditions of the Creative Commons Attribution (CC BY) license (http://creativecommons.org/licenses/by/4.0/).



REFERENCES

Ananda Kumari, R., Optical and SHG Measurements of Aminoacids doped ADP NLO crystals, *MRS Adv.*, 5, 1955–1963 (2020). https://doi.org/10.1557/adv.2020.265

Aslfattahi, N., Rahman, S., Mohd Sabri, M. F. and Arifutzzaman, A., Experimental Investigation of Thermal Stability and Enthalpy of Eutectic Alkali Metal Solar Salt Dispersed with MgO Nanoparticles, *Int. J. Technol.*, 10(6), 1112 (2019). https://doi.org/10.14716/ijtech.v10i6.3568

Atinafu, D. G., Yun, B. Y., Yang, S. and Kim, S., Encapsulation of dodecane in gasification biochar for its prolonged thermal/shape stability, reliability, and ambient enthalpy storage, *Chem. Eng. J.*, 437, 135407 (2022). https://doi.org/10.1016/j.cej.2022.135407

Sahaya, B. I. L., Muthu, S. P., P., K., B., G. and P., R., Synthesis, crystal growth and characterization of organic 1,2,4-triazole p-nitrophthalic acid (TPNP) single crystal for nonlinear optical (NLO) applications, *Inorg. Chem. Commun.*, 158, 111549 (2023). https://doi.org/10.1016/j.inoche.2023.111549

Bassett, L. C., Alkauskas, A., Exarhos, A. L. and Fu, K.-M. C., Quantum defects by design, *Nanophotonics*, 8(11), 1867–1888 (2019). https://doi.org/10.1515/nanoph-2019-0211

Chakaravarthy, R., Tao, J., Liu, C., Liu, Y., Ren, W. andEzhil Vizhi, R., Potassium trihydrogen dioxalate dihydrate (KTO) nonlinear optical (NLO) single crystal for optical limiting application, *Results Phys.*, 51, 106732 (2023). https://doi.org/10.1016/j.rinp.2023.106732

Chandra Kandpal, B., Gupta, D. K., Kumar, A., Kumar Jaisal, A., Kumar Ranjan, A., Srivastava, A. and Chaudhary, P., Effect of heat treatment on properties and microstructure of steels, *Mater. Today Proc.*, 44, 199–205 (2021). https://doi.org/10.1016/j.matpr.2020.08.556

Durgababu, G., Swati, G., Vijayan, N., Maurya, K. K., Kamalesh, T., Nagaraju, G. J. and Bhagavannarayana, G., Influence of l-Phenylalanine doping on potassium dihydrogen phosphate: crystal growth, structural, optical and mechanical traits, *J. Mater. Sci. Mater. Electron.*, 32(5), 5698–5712 (2021). https://doi.org/10.1007/s10854-021-05291-0

Feng, Y., Lin, S., Huang, S., Shrestha, S. and Conibeer, G., Can Tauc plot extrapolation be used for direct-band-gap semiconductor nanocrystals?, *J. Appl. Phys.*, 117(12), 1–15 (2015). https://doi.org/10.1063/1.4916090

Gu, B., Cavaletto, S. M., Nascimento, D. R., Khalil, M., Govind, N. and Mukamel, S., Manipulating valence and core electronic excitations of a transition-metal complex using UV/Vis and X-ray cavities, *Chem. Sci.*, 12(23), 8088–8095 (2021). https://doi.org/10.1039/D1SC01774H

Henning, F. G., Schnitzler, E., Demiate, I. M., Lacerda, L. G., Ito, V. C., Malucelli, L. C. and da Silva Carvalho Filho, M. A., Fortified Rice Starches: The Role of Hydrothermal Treatments in Zinc Entrapment, *Starch - Stärke*, 71(1–2), 1–8 (2018). https://doi.org/10.1002/star.201800130

Ilbay, S. G., Güvener, S. and Alkumru, H. N., Processing dentures using a microwave technique, *J. Oral Rehabil.*, 21(1), 103–109 (1994). https://doi.org/10.1111/j.13652842.1994.tb01129x

Jubu, P. R., Yam, F. K., Igba, V. M. and Beh, K. P., Tauc-plot scale and extrapolation effect on bandgap estimation from UV–vis–NIR data – A case study of β-Ga2O3, *J. Solid State Chem.*, 290, 121576 (2020). https://doi.org/10.1016/j.jssc.2020.121576

Kiran, Vijayan, N., Sarkar, N., Joshi, D., Jyoti, Kumar, K., Yadav, S. and Das, S., Unveiling the optical, thermal and nonlinear behavior of guanidinium benzenesulfonate: A promising organic single crystal for NLO applications, *Opt. Mater. (Amst).*, 147, 114683 (2024). https://doi.org/10.1016/j.optmat.2023.114683

Klein, J., Kampermann, L., Mockenhaupt, B., Behrens, M., Strunk, J. and Bacher, G., Limitations of the Tauc Plot Method, *Adv. Funct. Mater.*, 33, 1–19 (2023). https://doi.org/10.1002/adfm.202304523

Li, X., Wu, F., Yao, Y., Wu, W., Ji, C., Li, L., Sun, Z., Luo, J. and Liu, X., Robust Spin-Dependent Anisotropy of Circularly Polarized Light Detection from Achiral Layered Hybrid Perovskite Ferroelectric Crystals, *J. Am. Chem. Soc.*, 144(31), 14031–14036 (2022). https://doi.org/10.1021/jacs.2c06048

Matsui, T., Tsujikawa, K., Imai, T., Akage, Y., Sakamoto, T., Hanzawa, N., Sagae, Y., Nakajima, K. and Morimura, H., Optical Fiber and Optical Device Technology for Innovative Manufacturing, *NTT Tech. Rev.*, 17(6), 41–44 (2019). https://doi.org/10.53829/ntr201906fa12

Matthias, B. and von Hippel, A., Domain Structure and Dielectric Response of Barium Titanate Single Crystals, *Phys. Rev.*, 73(11), 1378–1384 (1948). https://doi.org/10.1103/PhysRev.73.1378

Purushothaman, P., Gopathy, R., Raju, E., Durairaj, N., Kandhan, S. and Mani, G., Structural, linear and nonlinear optical, electrical and NBO reports on 4-aminopyridine-1-ium 4-aminobenzoate single crystal for SHG, optoelectronics and violet laser emission applications, *J. Mater. Sci. Mater. Electron.*, 32(17), 22342–22361 (2021). https://doi.org/10.1007/s10854-021-06720-w

Purusothaman, R., Shankar, M., Dennis Raj, A., Vimalan, M. and Vetha Potheher, I., A study on NLO, ultraviolet transparency, photoconductivity, and dielectric response of organic single crystal, *J. Mater. Sci. Mater. Electron.*, 34(36), 2292 (2023). https://doi.org/10.1007/s10854-023-11691-1

Ramesh, V., Third order nonlinear materials of: L–threonine hydrochloride and zinc chloride doped L – threonine hydrochloride, *Mater. Today Proc.*, 33, 4044–4046 (2020). https://doi.org/10.1016/j.matpr.2020.06.429

Rao, E. N., Vaitheeswaran, G., Reshak, A. H. and Auluck, S., Effect of lead and caesium on the mechanical, vibrational and thermodynamic properties of hexagonal fluorocarbonates: a comparative first principles study, *RSC Adv.*, 6(102), 99885–99897 (2016). https://doi.org/10.1039/C6RA20408B

Rao, V., Singh, P. K. and Dwivedi, D. K., Effect of third element on thermo-mechanical properties of Se-Te-M (M= Ge, Sb) glassy alloys: A comparatively study, In: AIP Conference Proceedings, p 120002 (2020). https://doi.org/10.1063/5.0001767

Sánchez, T. J. L., Marzoa, V., Bernardo-Gavito, R., Pau, J. L. and Granados, D., Hands-On Quantum Sensing with NV− Centers in Diamonds, *C- J. Carbon Res.*, 9(1), 16 (2023). https://doi.org/10.3390/c9010016

Shi, Z., Wang, Y., Xiao, T., Dong, S. and Lan, T., Preparation and Thermal Decomposition Kinetics of a New Type of a Magnetic Targeting Drug Carrier, *ACS Omega*, 6(4), 3427–3433 (2021). https://doi.org/10.1021/acsomega.0c06075

Tailor, N. K., Maity, P., Saidaminov, M. I., Pradhan, N. and Satapathi, S., Dark Self-Healing-Mediated Negative Photoconductivity of a Lead-Free Cs 3 Bi 2 Cl 9 Perovskite Single Crystal, *J. Phys. Chem. Lett.*, 12(9), 2286–2292 (2021). https://doi.org/10.1021/acs.jpclett.1c00057

Tian, H., Lin, C., Zhao, X., Xu, F., Wang, C., Ye, N. and Luo, M., Ba(SO 3 CH 3) 2 : A Deep-Ultraviolet Transparent Crystal with Excellent Optical Nonlinearity Based on a New Polar Non-π-Conjugated NLO Building Unit SO 3 CH 3 −, *CCS Chem.*, 5(11), 2497–2505 (2023). https://doi.org/10.31635/ccschem.023.202202582

Wang, D., Meng, X., Zhang, N., Sun, D., Hou, R., Chen, H. and Liu, X., Characteristics of structure, thermal stability and optical properties for a novel NLO crystal (C5H12NO)H2PO4, *Opt. Mater. (Amst).*, 135, 113225 (2023). https://doi.org/10.1016/j.optmat.2022.113225

Wang, J. and Dong, J., Optical Waveguides and Integrated Optical Devices for Medical Diagnosis, Health Monitoring and Light Therapies, *Sensors*, 20(14), 3981 (2020). https://doi.org/10.3390/s20143981

Yauri, R., Gamero, V. and Alayo, M., Characterization of the electrical properties of an optical device manufactured with CMOS 0.35 μm technology, *Indones. J. Electr. Eng. Comput. Sci.*, 32(3), 1346 (2023). https://doi.org/10.11591/ijeecs.v32.i3.pp1346-1352

Zallo, E., Pianetti, A., Prikhodko, A. S., Cecchi, S., Zaytseva, Y. S., Giuliani, A., Kremser, M., Borgardt, N. I., Finley, J. J., Arciprete, F., Palummo, M., Pulci, O. and Calarco, R., Two-dimensional single crystal monoclinic gallium telluride on silicon substrate via transformation of epitaxial hexagonal phase, *npj 2D Mater. Appl.*, 7(1), 19 (2023). https://doi.org/10.1038/s41699-023-00390-4